Large Internal Variability Dominates over Global Warming Signal in Observed Lower Stratospheric QBO Amplitude

AARON MATCH[a] AND STEPHAN FUEGLISTALER[a,b]

[a] *Program in Atmospheric and Oceanic Sciences, Princeton University, Princeton, New Jersey*
[b] *Department of Geosciences, Princeton University, Princeton, New Jersey*

(Manuscript received 5 April 2021, in final form 15 September 2021)

ABSTRACT: Global warming projections of dynamics are less robust than projections of thermodynamics. However, robust aspects of the thermodynamics can be used to constrain some dynamical aspects. This paper argues that tropospheric expansion under global warming (a thermodynamical process) explains changes in the amplitude of the quasi-biennial oscillation (QBO) in the lower and middle stratosphere (a dynamical process). A theoretical scaling for tropospheric expansion of approximately 6 hPa K^{-1} is derived, which agrees well with global climate model (GCM) experiments. Using this theoretical scaling, the response of QBO amplitude to global warming is predicted by shifting the climatological QBO amplitude profile upward by 6 hPa per kelvin of global warming. In global warming simulations, QBO amplitude in the lower to middle stratosphere shifts upward as predicted by tropospheric expansion. Applied to observations, the tropospheric expansion framework suggests a historical weakening of QBO amplitude at 70 hPa of 3% $decade^{-1}$ from 1953 to 2020. This expected weakening trend is half of the 6% $decade^{-1}$ from 1953 to 2012 detected and attributed to global warming in a recent study. The previously reported trend was reinforced by record low QBO amplitudes during the mid-2000s, from which the QBO has since recovered. Given the modest weakening expected on physical grounds, past decadal modulations of QBO amplitude are reinterpreted as a hitherto unrecognized source of internal variability. This large internal variability dominates over the global warming signal such that, despite 65 years of observations, there is not yet a statistically significant weakening trend.

KEYWORDS: Quasibiennial oscillation; Tropopause; Climate change; Climate models; Internal variability

1. Introduction

In climate models, future projections of thermodynamical variables (those controlled by global average surface temperature) are more robust than future projections of dynamical variables (those controlled by the circulation) (Shepherd 2014). Thermodynamical variables include specific humidity and tropospheric temperature. Dynamical variables include changes in the atmospheric circulation, such as the midlatitude jet and precipitation patterns. The lack of robustness in future projections of many dynamical variables slows efforts to confidently project future changes in variables of societal relevance, such as storm tracks and regional precipitation.

However, some future projections of dynamical variables are quite robust. For example, the residual mean circulation in the lower stratosphere (the Brewer–Dobson circulation) is a dynamical variable, as it is driven by the dissipation of atmospheric waves (e.g., Butchart 2014), yet projections of future strengthening of the residual mean circulation in the lower stratosphere are quite robust (Butchart and Scaife 2001; Butchart et al. 2006). This strengthening has been explained in terms of changes in wave driving (Garcia and Randel 2008; Shepherd and McLandress 2011), which, although accurate, suggests a tension between the robustness of the model results and the nonrobustness that typically accompanies explanations of comparable dynamical complexity. This strengthening has also been explained in thermodynamical terms as a simple consequence of tropospheric expansion under global warming, which seems consistent with the noted robustness of these changes (Oberländer-Hayn et al. 2016).

Tropospheric expansion amounts to a shift in perspective: rather than thinking of global warming as leading to a temperature increase on a given pressure level, global warming can equivalently be considered as a vertical shift of temperatures—and their associated dynamical and microphysical features—in pressure space. Tropospheric expansion is well recognized (see also Vallis et al. 2015) and has been used to construct a robust thermodynamical constraint for vertical shifts due to global warming in dynamical, microphysical, and cloud-related quantities (Tompkins and Craig 1999; Lorenz and DeWeaver 2007; Singh and O'Gorman 2012).

In this paper, we develop a theoretical scaling for tropospheric expansion that facilitates quantitative predictions for changes in atmospheric dynamics in the upper troposphere and lower stratosphere. We apply this theoretical scaling to interpret variability and trends in the amplitude of the quasi-biennial oscillation (QBO). The QBO is the dominant mode of dynamical variability in the tropical stratosphere, featuring a pattern of alternating zonal mean zonal winds with a period of roughly 28 months. The QBO is driven by atmospheric waves triggered by convection in the underlying troposphere. The amplitude of the QBO can be measured as the standard deviation of the zonal-mean zonal winds, possibly after applying filters in time or subtracting the seasonal cycle (e.g., Dunkerton and Delisi 1985). QBO

Corresponding author: Aaron Match, amatch@princeton.edu

DOI: 10.1175/JCLI-D-21-0270.1

amplitude maximizes between 10 and 20 hPa, and drops off gradually through the lower stratosphere before vanishing into the background below the 70-hPa level.

Recently, interest has grown in how the amplitude of the QBO responds to global warming. Kicking off such interest in QBO amplitude trends, Kawatani and Hamilton (2013, hereafter KH13) reported that the QBO at 70 hPa was weakening by 6% (±3%) decade^{-1} based on radiosonde wind observations during the period 1953–2012. The linear trend from 1953 to 2012 corresponded to a weakening of the QBO at 70 hPa by a factor of one-third. This weakening trend was found to be consistent in sign with expectations from global warming experiments in global climate models (GCMs), which predict a weakening of the QBO at the 70-hPa level as well as aloft into the midstratosphere. Observed weakening trends are not evident aloft (see also Richter et al. 2020; Butchart et al. 2020).

The 70-hPa level (where weakening has been simulated and observed) sits at the top of the QBO *buffer zone*, the region within which the QBO vanishes despite sufficient wave stress to drive the oscillation (Match and Fueglistaler 2019). The buffer zone has previously been understood to be formed by residual mean upwelling, based on the results of Saravanan (1990). KH13 argued that the weakening of the QBO could be interpreted as a deepening of the buffer zone due to the expected strengthening of the residual mean upwelling as a result of global warming. Because direct measurements of residual mean upwelling remain inaccessible, KH13 proposed that trends in the QBO could constrain the trends in residual mean upwelling.

Since the publication of KH13, several events have occurred that motivate revisiting trends in QBO amplitude. First, QBO amplitude has returned to its long-term average after a mid-2000s minimum, motivating an updated calculation of the trend and its consequent detection and attribution statements. Second, the causal model adopted in KH13 to understand the formation of the buffer zone—the *upwelling hypothesis*—has been found to rely in a logically circular way on the prescribed lower boundary condition of the classical model of the QBO (Match and Fueglistaler 2020). A revised causal model has been proposed—the *mean flow damping hypothesis*—emphasizing the role of horizontal eddy momentum flux divergence in damping the QBO to form the buffer zone (Match and Fueglistaler 2019). Third, in contrast to the typical nonrobustness of dynamical changes in global warming experiments, as discussed in Shepherd (2014), the robustness of simulated QBO weakening suggests a possible connection to robust thermodynamical changes. The relevant thermodynamical change could be tropospheric expansion, which has previously been shown to explain robust changes in residual mean upwelling in the upper troposphere and lower stratosphere (Oberländer-Hayn et al. 2016). The tropospheric expansion framework has not previously been applied to the QBO.

In section 2, we derive a scaling predicting 6 hPa of tropospheric expansion per kelvin of global average surface warming. The tropospheric expansion scaling is based on the assumption that the troposphere is moist adiabatic with constant near-surface relative humidity and an isothermal top. The tropospheric expansion scaling performs well in global warming experiments in a set of GCMs contributed to phase 6 of the Coupled Model Intercomparison Project (CMIP6). In section 3, we demonstrate that the QBO amplitude profile in the lower to middle stratosphere appears to shift upward in response to global warming. The upward shift is predicted by the tropospheric expansion scaling, which provides a quantitatively accurate prediction for QBO amplitude changes at 70 hPa. For the observed warming over the period 1953–2020, tropospheric expansion predicts a weakening trend of 3% decade^{-1} (half the weakening trend of 6% decade^{-1} reported in KH13 from 1953 to 2012). The smaller magnitude of the expected trend leads us to reinterpret the large observed variability in QBO amplitude as internal variability. Recognition of the large internal variability prompts a calculation showing that the observed weakening trend is not statistically significant, in contrast to previous results. In the discussion section (section 4), we discuss the implications of these results for interpreting whether QBO amplitude constrains residual mean upwelling in the tropical stratosphere. The large internal variability in QBO amplitude highlights a region (the tropics), phenomenology (the QBO), and frequency (decadal) of variability in stratospheric dynamics that is rarely emphasized in comparison to other well-studied sources of variability.

2. Tropospheric expansion

a. A simple analytical theory for tropospheric expansion

For the purposes of deriving a simple scaling for the rate of tropospheric expansion, the troposphere can be approximated as having uniform moist entropy. To relate moist entropy at the surface and top of the troposphere, we use the equivalent potential temperature [$\theta_e = \theta\exp(L_v q^*\phi/c_p T)$], with potential temperature $\theta = T(p_s/p)^{R/c_p}$, latent heat of vaporization $L_v = 2.5 \times 10^6\,\mathrm{J\,kg^{-1}}$, saturation specific humidity q^* (kg water vapor per kg dry air), relative humidity ϕ (dimensionless), specific heat capacity of air at constant pressure $c_p = 1004\,\mathrm{J\,kg^{-1}\,K^{-1}}$, temperature T (K), pressure p, and gas constant of air $R = 287\,\mathrm{J\,kg^{-1}\,K^{-1}}$. Subscript t refers to the top of the troposphere and s refers to the surface (e.g., p_s is surface pressure). Quantitatively, the approximate uniformity of moist entropy can be appreciated by noting that in the tropics (from 30°S to 30°N), the lowest 850 hPa of the atmosphere (from 1000 to 150 hPa) exhibits an equivalent potential temperature increase of only 25 K. By contrast, in the next 100 hPa (from 150 to 50 hPa), the equivalent potential temperature increases by about 130 K. Assuming that the top of the troposphere is approximately dry ($q_t^* \approx 0$) leads to the following expression for the equivalent potential temperature at the top of the troposphere:

$$\theta_{e,t} = T_t\left(\frac{p_s}{p_t}\right)^{R/c_p}. \tag{1}$$

Noting that the surface air is at surface pressure leads to the following expression for the equivalent potential temperature at the surface:

$$\theta_{e,s} = T_s \exp\left(\frac{L_v q_s^* \phi_s}{c_p T_s}\right). \tag{2}$$

Approximating the troposphere as having uniform moist entropy [i.e., setting Eqs. (1) and (2) equal to each other] yields the following expression for tropospheric depth Δp:

$$\Delta p = p_s - p_t = p_s\left[1 - \left(\frac{T_t}{T_s}\right)^{c_p/R}\exp\left(\frac{-L_v q_s^* \phi_s}{RT_s}\right)\right]. \quad (3)$$

We seek an expression for the zeroth-order rate of change of tropospheric depth as a function of global warming (i.e., $d\Delta p/dT_s$). To evaluate $d\Delta p/dT_s$, it is necessary to capture the physical dependence on T_s of each term in Eq. (3). Differentiating Eq. (3) with respect to T_s, assuming constant p_s, yields

$$\frac{d\Delta p}{dT_s} = (p_s - \Delta p)\left[\frac{c_p\left(1 - \frac{T_s}{T_t}\frac{dT_t}{dT_s}\right) + L_v\left(\phi_s\frac{dq_s^*}{dT_s} - \frac{q_s^*\phi_s}{T_s} + q_s^*\frac{d\phi_s}{dT_s}\right)}{RT_s}\right]. \quad (4)$$

The rate of change of tropospheric depth with respect to changes in surface temperature depends on the rate of change of temperature at the top of the troposphere, the rate of change of surface saturation specific humidity, and the rate of change of surface relative humidity. We can further simplify Eq. (4) for the case of greenhouse gas forcing by using physical expectations for the relationships of temperature, pressure, and moisture variables in the troposphere as a function of greenhouse gas–induced global warming. First, due to energetic constraints, tropospheric near-surface relative humidity over the oceans changes little with global warming (Boer 1993), so the term multiplied by $d\phi_s/dT_s$ is dominated by the term multiplied by dq_s^*/dT_s. Second, it has been noted in climate model simulations of varying complexities and explained based on the spectroscopic properties of water vapor that the temperature at the top of the troposphere should remain approximately fixed with global warming [the so-called fixed anvil temperature (FAT) or fixed tropopause temperature (FiTT) hypotheses] (Hartmann and Larson 2002; Kuang and Hartmann 2007; Seeley et al. 2019; Jeevanjee and Fueglistaler 2020) ($dT_t/dT_s \approx 0$). Indeed, the only derivative with respect to surface temperature on the right-hand side of Eq. (4) that is expected to be large is that of the surface saturation specific humidity q_s^*. We will assume that the surface saturation specific humidity q_s^* is set by the Clausius–Clapeyron relationship applied at T_s. Under the above assumptions, Eq. (4) reduces to the following:

$$\frac{d\Delta p}{dT_s} = (p_s - \Delta p)\left[\frac{c_p + L_v\phi_s\left(-\frac{q_s^*}{T_s} + \frac{dq_s^*}{dT_s}\right)}{RT_s}\right]. \quad (5)$$

Equation (5) shows the rate of change of tropospheric depth with warming. Since $p_s > \Delta p$ (i.e., the first term in parentheses is positive) and the term in the square brackets is dominated by positive contributions from its first and third terms, $d\Delta p/dT_s$ is positive and the troposphere deepens in pressure coordinates with global warming. Tropospheric deepening provides the decrease in pressure required to maintain constant temperature at the top of the troposphere as the surface drives increases in moist entropy. To gain some physical intuition regarding Eq. (5), consider that for a dry atmosphere ($\phi_s = 0$), the increase in moist entropy at the surface reduces to the increase in dry entropy associated with increasing the temperature. Inserting approximate parameters (T_s = 300 K, T_t = 200 K) yields a dry tropospheric depth (Δp) of 758 hPa [solved from Eq. (3)] and a rate of change of dry tropospheric depth with global warming $d\Delta p/dT_s$ of 2.8 hPa K^{-1}. For a moist atmosphere, the increase in moist entropy at the surface includes the dry component plus increases due to Clausius–Clapeyron scaling of moisture at the surface. Inserting approximate parameters of $\phi_s = 0.7$ and using the Clausius–Clapeyron equation to compute the moisture parameters ($q_s^* = 0.022$ and $dq_s^*/dT_s = 0.0014\,K^{-1}$) yields Δp = 847 hPa and $d\Delta p/dT_s$ = 5.8 hPa K^{-1}. Note that accounting for moisture for the present climate approximately doubles the estimated rate of tropospheric expansion.

In summary, the troposphere is expected to deepen by approximately 6 hPa per kelvin of warming. This estimate depends on the physical assumptions in the calculation and on the parameters chosen to represent the basic state, and should be treated as an approximate value. For example, the estimate is sensitive to plausible alternative choices for the temperature at the top of the troposphere, where T_t = 210 K yields Δp = 818 hPa and $d\Delta p/dT_s \approx 7$ hPa K^{-1}, and T_t = 190 K yields Δp = 872 hPa and $d\Delta p/dT_s \approx 5$ hPa K^{-1}.

b. *Tropospheric expansion in global climate models*

We evaluate the theoretical scaling for tropospheric depth in five GCMs that submitted simulations to CMIP6: CESM2-WACCM, CNRM-CM6-1, HadGEM3-GC31-LL, IPSL-CM6A-MR, and MIROC6. These models were chosen because they have internally generated QBOs and the necessary radiative heating rate diagnostics. (Later analysis of the QBO covers an additional seven CMIP6 models.) We use the preindustrial control (piControl) experiments to characterize the control state and the experiments with CO_2 increasing by 1% yr^{-1} for 150 years (1pctCO2) to evaluate the forced response to greenhouse gas warming. The 1pctCO2 experiments manifest a clear global warming signal in the evolution of tropospheric depth. We compare two proxies for tropospheric depth, which will be shown to agree with each other and with the theory for the rate of change of tropospheric depth in response to global warming. These proxies are evaluated in the tropics from 30°S to 30°N.

The first proxy is a column-integrated diagnostic that relies on the idea that the troposphere and stratosphere are distinguished insofar as the bulk of Earth's globally integrated total radiative cooling (longwave plus shortwave) occurs in the troposphere. The proxy $\Delta p_{99\%}$ defines tropospheric depth as the pressure depth beginning at the surface and extending up to the level that contains 99% of the column-integrated total radiative cooling. This diagnostic can be applied globally or just in the tropics; here it is applied in the tropics. Since the total radiative cooling of the atmosphere is roughly $-100\,W\,m^{-2}$

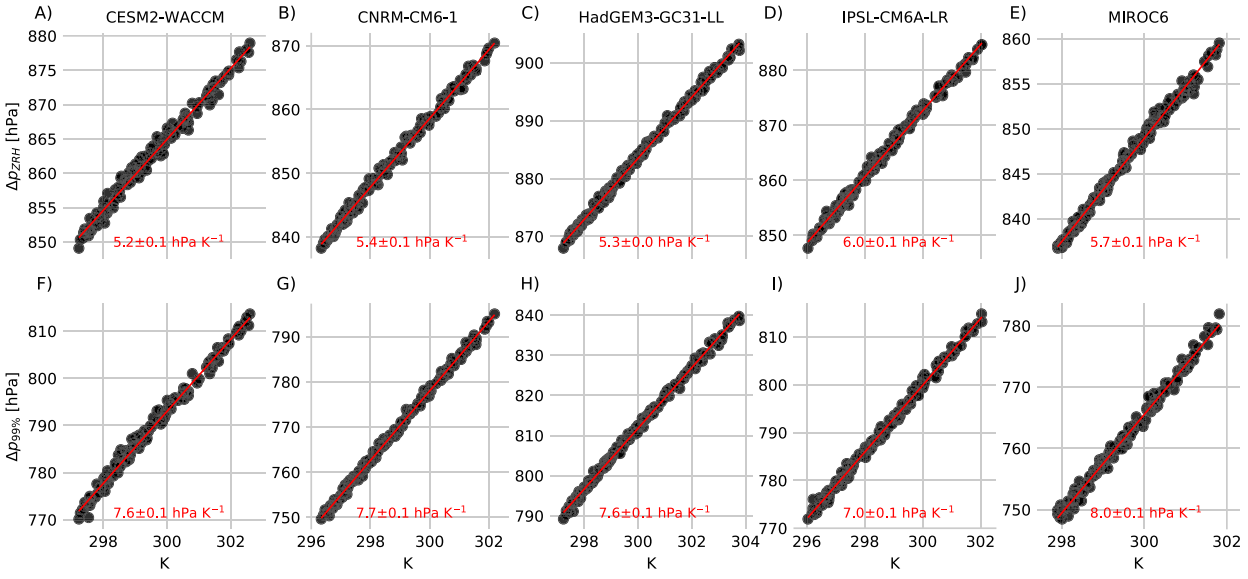

FIG. 1. Proxies of tropospheric depth vs average surface temperature in 1pctCO2 experiments: (a)–(e) Δp_{ZRH} (defined from surface to level of zero radiative heating) and (f)–(j) $\Delta p_{99\%}$ (defined as the pressure depth above the surface that contains 99% of the integrated radiative cooling). Data are averaged over the tropics from 30°S to 30°N. Uncertainty in the slope corresponds to the 95% confidence interval.

(which is primarily balanced by latent heating and to a lesser degree by sensible heating), the integrated radiative cooling outside $\Delta p_{99\%}$ is approximately $-1\ \mathrm{W\,m^{-2}}$; $\Delta p_{99\%}$ has a value of 800 ± 50 hPa in the 1pctCO2 experiments.

The second proxy is a diagnostic for the tropics only that relies on the idea that the tropical troposphere is cooling radiatively whereas the tropical stratosphere is heating radiatively. The proxy Δp_{ZRH} defines tropospheric depth as the pressure depth from the surface up to the level of zero radiating cooling in the vicinity of the tropopause (Δp_{ZRH} ranges from 850 to 900 hPa in the 1pctCO2 experiments).

These proxies measure different but related aspects of the radiative depth of the troposphere. They exhibit a mean offset, but this is not problematic because the main aim is to ascertain their slope with respect to global average surface temperature. Figure 1 shows scatterplots of these yearly tropospheric depth proxies as a function of temperature in the 1pctCO2 experiments. The rate of deepening is comparable for the two diagnostics (7.0–8.0 hPa $\mathrm{K^{-1}}$ for $\Delta p_{99\%}$ and 5.2–6.0 hPa $\mathrm{K^{-1}}$ for Δp_{ZRH}), which are both consistent with the theoretical scaling of 6 hPa $\mathrm{K^{-1}}$. Consistent with theory, the troposphere deepens with increasing global average surface temperature. Note that in evaluating these proxies, we do not make use of any of the assumptions outlined in the analytical scaling. Therefore, the GCM results constitute a test of the analytical scaling. The correspondence between the 1pctCO2 experiments and the theoretical scaling for different metrics gives confidence that tropospheric deepening is well described by the theoretical scaling.

c. *Tropospheric expansion in MERRA-2*

Tropospheric expansion was evaluated in the MERRA-2 atmospheric reanalysis, covering the period 1980–2020. For MERRA-2, we used the clear-sky radiative heating rates (Gelaro et al. 2017; GMAO 2015a,b). The tropospheric depth up to the level of zero radiative heating (Δp_{ZRH}) was found to vary approximately linearly with temperature with a slope of 8.6 ± 1.2 hPa $\mathrm{K^{-1}}$ (Fig. 2a); $\Delta p_{99\%}$ was found to be noisier, with a slope of 3.8 ± 2.0 hPa $\mathrm{K^{-1}}$. Despite some noise in the tropospheric depth metrics in MERRA-2, there is a detectable trend in both metrics (as indicated by the slopes significantly greater than zero at 95% confidence). Tropospheric expansion in MERRA-2 appears roughly consistent with the theoretical scaling of approximately 6 hPa $\mathrm{K^{-1}}$, although it is noted that 6 hPa $\mathrm{K^{-1}}$ lies outside the 95% confidence interval for both metrics.

3. QBO amplitude trends

a. *The buffer zone of the QBO*

Leveraging the robust thermodynamical constraint on tropospheric depth from the foregoing section, we evaluate trends in the amplitude of the QBO. To introduce the QBO, Fig. 3a shows a representative set of approximately four periods of the QBO from 2000 to 2010 with daily data from MERRA-2. The QBO manifests as alternating and descending zonal mean zonal winds with a period averaging 28 months (Baldwin et al. 2001).

Figure 3b shows the amplitude of the QBO. Following Dunkerton and Delisi (1985), KH13 measured QBO amplitude using a three-cycle running standard deviation of the zonal wind smoothed with a 5-month running average, with QBO cycles defined based on the wind reversals at 30 hPa. The 2016 disruption of the QBO temporarily reconfigured the phase relationships among levels of the QBO (Newman et al. 2016; Match and Fueglistaler 2021), rendering it problematic to define QBO cycles based on the wind at 30 hPa (or any single

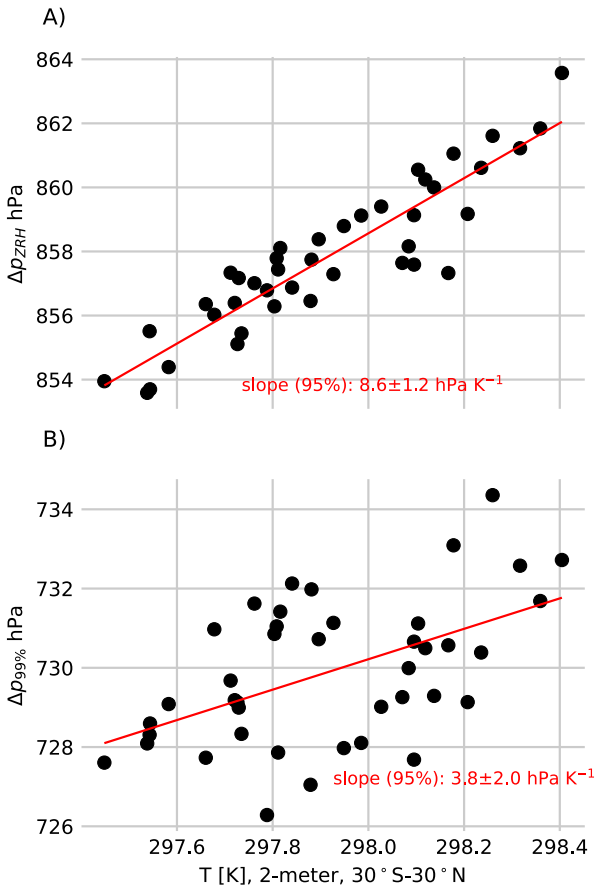

FIG. 2. Annual radiative metrics of tropospheric depth vs average surface temperature in MERRA-2 averaged from 30°S to 30°N: (a) Δp_{ZRH}, the level of zero radiative cooling in the vicinity of the tropopause, and (b) $\Delta p_{99\%}$, the pressure depth above the surface that contains 99% of the integrated radiative cooling. Uncertainty in the slope corresponds to the 95% confidence interval.

level). To circumvent this problem, we define here a metric that builds on Dunkerton and Delisi (1985) but is locally defined: the amplitude A is defined as the 72-month running standard deviation of the deseasonalized 5-month smoothed zonal wind. The amplitude time series produced using the metric defined here and the metric defined in Dunkerton and Delisi (1985) are well correlated and yield similar trend estimates.

Figure 3b illustrates that the QBO rapidly decays in amplitude before vanishing below 70 hPa. The vanishing of the QBO near 70 hPa is surprising because idealized models suggest that the QBO should descend down to the source of the vertically propagating waves that drive it, which occurs at altitudes at or below 150 hPa. The region where the QBO amplitude vanishes despite sufficient wave stress to drive a QBO is known as the buffer zone. Previously, the buffer zone was understood to be formed by residual mean upwelling, which opposed the descent of the QBO (Saravanan 1990). Based on the idea that residual mean upwelling forms the buffer zone, KH13 argued that increasing upwelling in the lower stratosphere due to global warming was weakening the QBO in the buffer zone. Yet, theoretical results reveal that the buffer zone cannot be formed by upwelling, but rather must be formed by mean flow damping (Match and Fueglistaler 2020). Empirical results implicate mean flow damping due to horizontal momentum flux divergence in forming the buffer zone (Match and Fueglistaler 2019).

b. *Quantifying QBO amplitude in response to tropospheric expansion: A_{shift}*

In light of these new theoretical results explaining the formation of the buffer zone, it is not obvious that residual mean upwelling plays a privileged role in forming the buffer zone or in buffer zone trends. Without needing to specify any particular mechanism that forms the buffer zone, we hypothesize that the entire complex of processes, including the source of waves that drive the QBO and all those processes that could hypothetically form the buffer zone, are shifting upward in concert. Given that the QBO amplitude increases with height in the lower stratosphere, an upward shift of the buffer zone leads to a decrease of the QBO amplitude on fixed pressure levels in the lower to middle stratosphere. The following equation provides a recipe for estimating QBO amplitude by representing tropospheric expansion as a shift along a reference QBO amplitude profile:

$$A_{\mathrm{shift}}(t,p) = \overline{A}[p + \delta p_{\mathrm{shift}}(t)], \tag{6}$$

where $A_{\mathrm{shift}}(t, p)$ is the QBO amplitude at a given time t and pressure level p predicted to result from a shift of size $\delta p_{\mathrm{shift}}(t)$ along the climatological vertical structure of QBO amplitude $\overline{A}(p)$. The overline indicates a reference value (or profile) that is constant in time and is derived from theory, observations, and/or a model control experiment. (We have adopted the δ notation to indicate the difference between the global warming and control states, e.g., $\delta p_{\mathrm{shift}}$, to disambiguate from the tropospheric depth in the mean state Δp.) The shift due to tropospheric expansion $\delta p_{\mathrm{shift}}(t)$ is calculated from the tropospheric expansion theory based on the global average temperature change as follows:

$$\delta p_{\mathrm{shift}}(t) = \frac{\overline{d\Delta p}}{dT_s}\delta T_s(t), \tag{7}$$

where $\overline{d\Delta p/dT_s}$ is a constant taken from the tropospheric expansion theory in section 2 to be 6 hPa K^{-1}, and $\delta T_s(t)$ is the global average surface temperature anomaly. Note that in computing $A_{\mathrm{shift}}(t, p)$, the only variable required from the warmed state is the global average surface temperature as a function of time $[\delta T_s(t)]$. Therefore, the tropospheric expansion theory provides a framework for predicting QBO amplitude "out of sample," in the sense that it does not require as inputs any QBO properties from the warmed state.

c. *Simulated QBO amplitude compared to A_{shift}*

We evaluate QBO amplitude trends within each of 12 CMIP6 GCMs and compare them to the trends predicted within the tropospheric expansion framework [i.e., we compare $A(t,p)$ with $A_{\mathrm{shift}}(t, p)$ as calculated in Eqs. (6) and (7)]. There are three

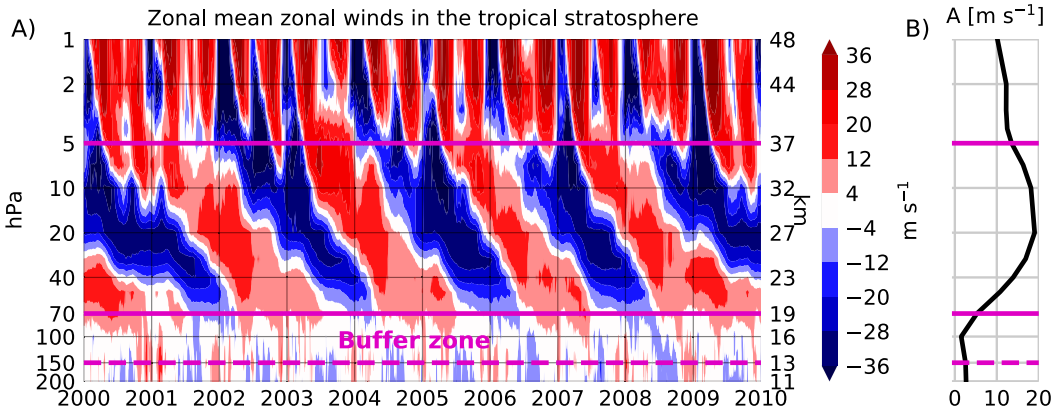

FIG. 3. (a) Zonal mean zonal winds of the QBO over the representative set of approximately four periods from 2000 to 2010. Data are from MERRA-2 at the equator. The left *y* axis shows the pressure, and the right *y* axis shows the approximate log-pressure height. The approximate bounds of the active QBO region (often identified as 70–5 hPa) are indicated by the solid magenta lines. The approximate bottom of the buffer zone (the region with vanishing QBO amplitude despite sufficient wave stress to drive a QBO, located roughly from 150 to 70 hPa; Match and Fueglistaler 2019) is indicated by the magenta dashed line. (b) QBO amplitude $A(p)$ (m s^{-1}) measured as the 72-month rolling standard deviation of the deseasonalized 5-month smoothed zonal wind and averaged in time across the MERRA-2 record from 1980 to 2020.

variables needed to compute $A_{\text{shift}}(t, p)$: $\overline{d\Delta p/dT_s}$, $\overline{A}(p)$, and $\delta T_s(t)$. We assume a constant rate of tropospheric expansion as a function of surface temperature $\overline{d\Delta p/dT_s} = 6\,\text{hPa K}^{-1}$, per section 2. We compute the climatological vertical structure of QBO amplitude $\overline{A}(p)$ and the global average surface temperature anomaly $\delta T_s(t)$ within each model, and the results are shown in Fig. 4 for the same five CMIP6 models used to analyze tropospheric expansion plus seven additional models. (The list of all CMIP6 models analyzed henceforth is as follows: AWI-CM-1-1-MR, BCC-CSM2-MR, CESM2-WACCM, CNRM-CM6-1, E3SM-1-0, EC-Earth3, GFDL-ESM4, HadGEM3-GC31-LL, IPSL-CM6A-LR, MIROC6, MPI-ESM1-2-HR, and MRI-ESM2-0.) Figure 4a shows $\overline{A}(p)$, computed from the time-averaged QBO amplitude in each piControl experiment. (The method for calculating QBO amplitude was described in section 3a.) Compared to MERRA-2, CMIP6 models generally underestimate QBO amplitude in the lower stratosphere (i.e., the buffer zone in CMIP6 models is too deep), which represents a persistent bias across model generations (e.g., Schenzinger et al. 2017; Richter et al. 2020). Figure 4b shows $\delta T_s(t)$, calculated as the global average surface temperature smoothed with a 72-month running average in each 1pctCO2 experiment minus the time-averaged global average surface temperature in the corresponding piControl experiment. Because models have different climate sensitivities, the GCMs exhibit different warming over time despite identical prescribed CO_2 concentrations. Correspondingly, models with stronger warming will have larger tropospheric expansion rates with time.

Using the variables presented in Fig. 4, we compute $A_{\text{shift}}(t, p)$ and compare it to the simulated QBO amplitude $A(t, p)$. The results are shown in Fig. 5. For each model, Fig. 5 shows a pair of contour plots: the top is $A(t, p)$, and the bottom is $A_{\text{shift}}(t, p)$. The QBO amplitude for a shift due to tropospheric expansion is calculated by linear interpolation in pressure along each model's climatological amplitude profile $\overline{A}(p)$ from Fig. 4a. In Fig. 5, the simulation panels show that the QBO appears to be ascending in all models. Whereas previous interpretations of QBO amplitude changes emphasized that the QBO was weakening in place, these figures emphasize that the QBO amplitude profile is ascending. The rate of ascent and corresponding QBO amplitude trends at any given level appear to be reasonably reproduced by $A_{\text{shift}}(t, p)$, although the agreement is stronger at 70 hPa but degrades at higher altitudes into the midstratosphere (e.g., 30 hPa).

The tropospheric expansion argument is expected to be most accurate at the bottom of the QBO domain and less accurate aloft. We expect reduced accuracy of tropospheric expansion aloft for the three reasons listed below. First, the vertical structure aloft can be governed by processes unrelated to the thermodynamical constraints relevant to tropospheric expansion. For example, ozone photochemistry exerts a leading-order control on stratospheric structure, and classical models of ozone photochemistry suggest that its vertical structure is approximately fixed in pressure (rather than fixed relative to the tropopause) (Chapman 1930). Second, the predictions of tropospheric expansion become absurd as the total pressure approaches the change predicted by tropospheric expansion. For example, it would be absurd to suggest that features near the stratopause at 1 hPa could shift upward by 6 hPa (to unphysical negative pressures). Third, the internal dynamics of the QBO could modulate its response to global warming in the interior of the domain in a manner that does not satisfy the expectations of tropospheric expansion.

As the tropospheric expansion framework is not expected to apply deep into the stratosphere, we next focus on evaluating the accuracy of A_{shift} where it is expected to apply most strongly—in the buffer zone of the QBO. Figure 6 compares

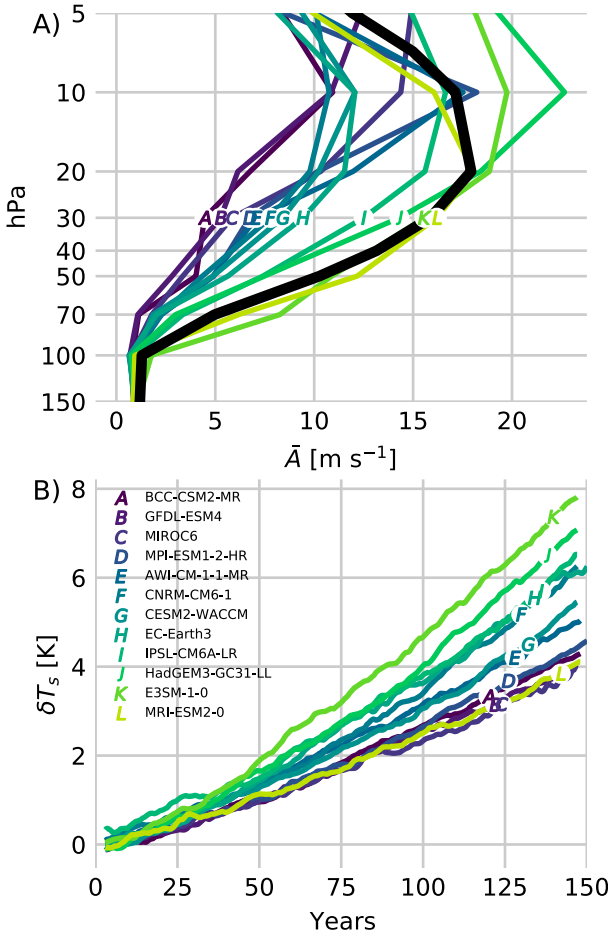

FIG. 4. Variables used to calculate $A_{\text{shift}}(t, p)$ with Eqs. (6) and (7). (a) Climatological (time-averaged) QBO amplitude $\overline{A}(p)$ in MERRA-2 from 1980 to 2020 (thick black line) and CMIP6 piControl simulations (colored lines). QBO amplitude is computed using the zonal mean zonal winds averaged from 5°S to 5°N. (b) Global average temperature anomaly $\delta T_s(t)$ in CMIP6 1pctCO2 experiments compared to the time average of the piControl experiment.

$A(t, 70\text{ hPa})$ with $A_{\text{shift}}(t, 70\text{ hPa})$. Figure 6 can be thought of as a horizontal slice at 70 hPa of Fig. 5. Note that $A_{\text{shift}}(t, 70\text{ hPa})$ is seen to provide a strong prediction for the long-term trends in $A(t, 70\text{ hPa})$. In particular, QBO amplitude exhibits decreasing trends in all GCMs, but at different rates. These different rates are quantitatively predicted using $A_{\text{shift}}(t, 70\text{ hPa})$. Interpreting these different rates in terms of the tropospheric expansion framework suggests that they can be explained by the climatological QBO amplitude profile and the rate of warming.

A curious feature of Fig. 6 is that the slope of $A_{\text{shift}}(t, 70\text{ hPa})$ appears to change discontinuously in some GCMs. Although the slope depends on the rate of warming, the discontinuities in slope do not arise from changes in the rate of warming. The discontinuities arise from the linear interpolation along $\overline{A}(p)$ used to compute the new QBO amplitude after applying δp_{shift}. The standardized pressure levels relevant to the linear interpolation in this problem occur at 150, 100, and 70 hPa. For the prediction of the amplitude at 70 hPa in the warmer climate, the base profile is initially evaluated (with linear interpolation) at a pressure between 70 and 100 hPa. However, when the global warming exceeds +5 K (as is the case for CESM2-WACCM, CNRM-CM6-1, E3SM-1-0, EC-Earth3, HadGEM3-GC31-LL, and IPSL-CM6A-LR), the shift exceeds 30 hPa and the base profile is evaluated between 100 and 150 hPa. The discontinuity in the evaluated slope is responsible for the change in the rate of change of QBO amplitude at 70 hPa with time in these models (Fig. 6). The discontinuity in the interpolating slope raises questions about how best to interpolate on the climatological QBO amplitude profile. The justification for an interpolation algorithm can depend in part on the physical priors that one has for the behavior of the function between the sampled points. For coarsely sampled functions (as in this case), higher-order spline interpolation can assert smoothness of derivatives, but at a cost of significant assumptions about the structure of the QBO amplitude profile between the sampled points. Quadratic and cubic interpolation did not appear to improve on the fit provided by the linear interpolation, so we present only the results from linear interpolation.

Although the tropospheric expansion theory provides a good prediction of the long-term trends in QBO amplitude, the simulated amplitude $A(t, p)$ exhibits substantial variability relative to its long-term trend. Over decadal periods, the QBO can appear to have the opposite trend to its true long-term trend. These deviations are interpreted as internal variability in QBO amplitude unrelated to global warming, the importance of which will be discussed below in section 3e.

d. *Observed QBO amplitude compared to A_{shift}*

We now compare observed QBO amplitude $A(t, p)$ with the prediction from tropospheric expansion $A_{\text{shift}}(t, p)$. The observed QBO amplitude $A(t, p)$ is calculated from radiosonde observations of zonal wind from 1953 to the present using the Freie Universität Berlin (FU-Berlin) dataset, which merges records from several stations in the tropics, in particular Singapore from 1976 to present. The FU-Berlin dataset has become a standard QBO observational metric and was also used in KH13. The global average surface temperature anomaly $\delta T_s(t)$ is calculated using the Berkeley Earth global average surface temperature, subtracting the time average over the MERRA-2 period (1980–2020). Because there is no control run for the observed QBO, $\overline{A}(p)$ must be computed from QBO properties that overlap in time with those predicted through the tropospheric expansion framework. The FU-Berlin dataset does not extend below the 70-hPa level (except over a smaller subset of the time period), so to facilitate interpolation below the 70-hPa level we use MERRA-2 to calculate $\overline{A}(p)$. We calculate $\overline{A}(p)$ as the time-averaged QBO amplitude in MERRA-2 over the period 1980–2020 using the equatorial zonal mean zonal winds. The resulting profile can be found in Fig. 3b.

Figure 7 shows the results, with the top panel depicting A and the bottom panel depicting A_{shift}. With approximately 1 K of global mean surface warming observed during the FU-Berlin time period, the QBO is predicted to have shifted by

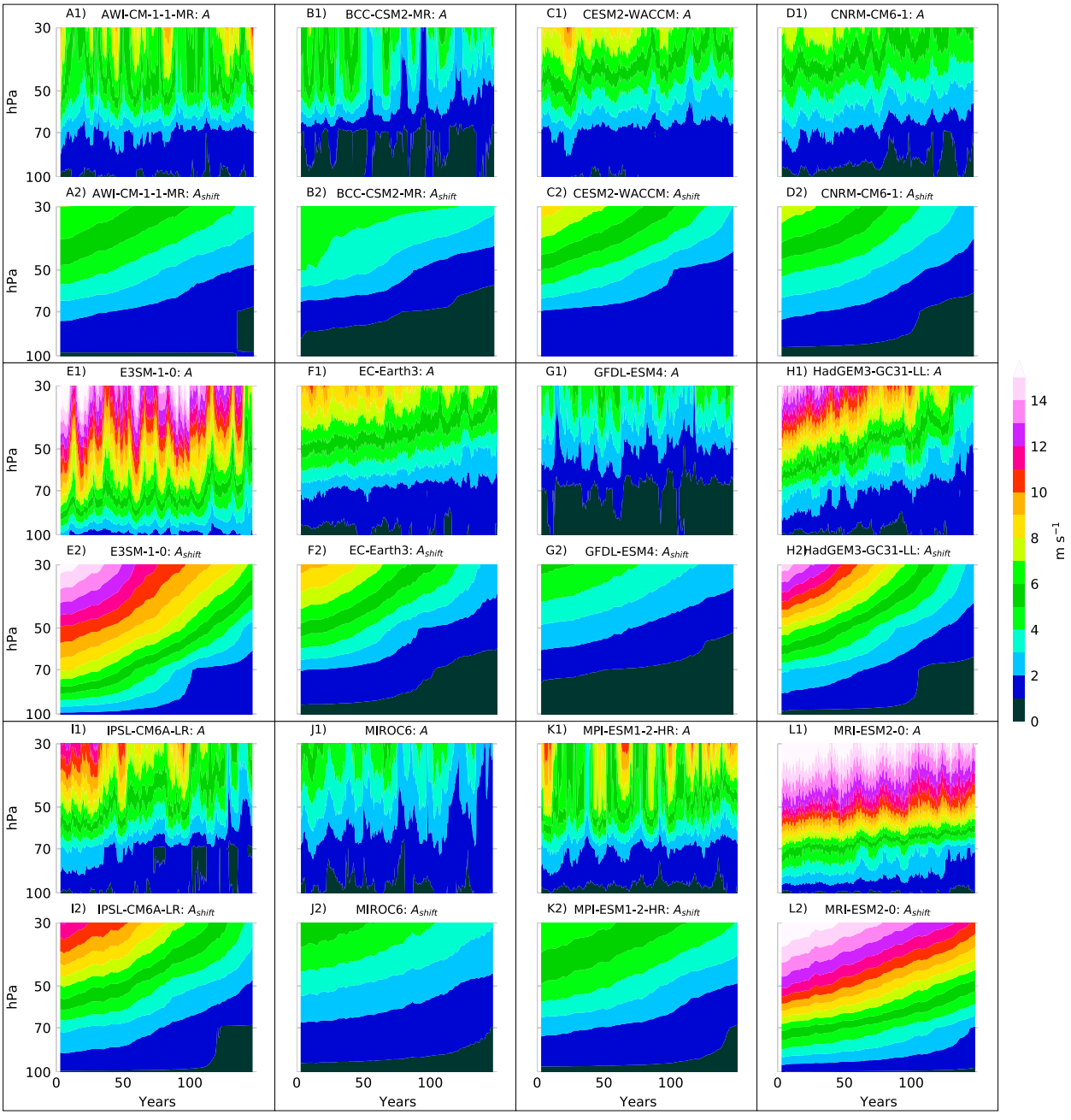

FIG. 5. QBO amplitude A simulated in CMIP6 1pctCO2 experiments (top of each pair, labeled "1") compared to A_{shift} calculated based on theory in Eqs. (6) and (7) and the model output in Fig. 4 (bottom of each pair, labeled "2"). The A_{shift} is calculated via linear interpolation along the climatological QBO amplitude $\overline{A}$ from the piControl experiment; A_{shift} predicts QBO amplitude trends in the lower stratosphere and even up toward the midstratosphere.

approximately 6 hPa during that period, as shown in Fig. 7b. The visual effects of the expected shift in Fig. 7b are subtle compared to the observed variability in Fig. 7a. The observations do not show striking evidence of a long-term upward shift.

Figure 8 focuses attention on QBO trends at 70 hPa. Figure 8a shows the zonal wind at 70 hPa in the FU-Berlin dataset, and compares it for reference to the equatorial zonal mean zonal winds in MERRA-2. (MERRA-2 assimilates the radiosonde wind observations that constitute the FU-Berlin dataset, so substantial agreement between the two datasets is to be expected and does not independently validate MERRA-2.) Figure 8b shows the QBO amplitude calculated from the FU-Berlin zonal wind, the MERRA-2 zonal wind, and $A_{\text{shift}}(t,$ 70 hPa). The QBO amplitude calculated from MERRA-2 agrees well with the amplitude computed in FU-Berlin after 2008, but the agreement is worse before 2008. A notable

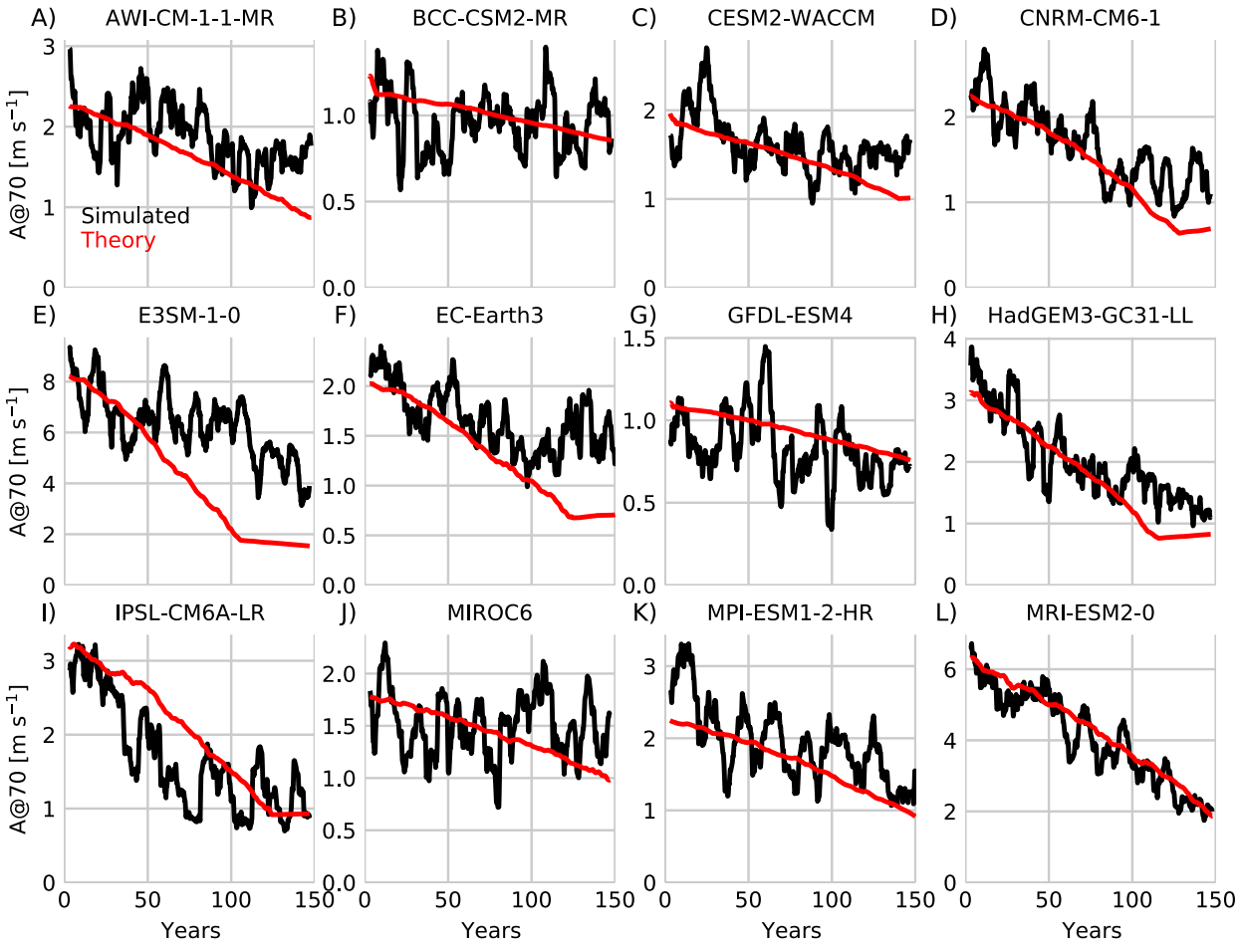

FIG. 6. QBO amplitude trends at 70 hPa sliced from Fig. 5. A_{shift} reproduces long-term trends at 70 hPa. Discontinuities in the slope of A_{shift} can arise when δp_{shift} exceeds the spacing between pressure levels, which occurs when δp_{shift} exceeds 30 hPa (i.e., $\delta T_s = 5$ K at $d\Delta p/dT_s = 6$ hPa K^{-1}) such that the linear interpolation changes from occurring between 70 and 100 hPa to occurring between 100 and 150 hPa.

difference is that the FU-Berlin dataset has a global minimum in the mid-2000s, whereas MERRA-2 has comparably low values in the mid-2000s and around 1990. The MERRA-2 record is not long enough to support an independent trend calculation, but the differences in QBO amplitude between MERRA-2 and FU-Berlin before 2008 despite similar underlying wind time series in Fig. 8a indicate that the QBO amplitude metric is sensitive to small differences in wind. We implicitly account for the sensitivity of the QBO amplitude metric later in a bootstrapping-based calculation of the significance of the observed trends.

Also shown in Fig. 8b is $A_{\text{shift}}(t, 70\text{ hPa})$, which is a horizontal slice at 70 hPa from Fig. 7b. The long-term weakening trend predicted by $A_{\text{shift}}(t, 70\text{ hPa})$ is 3% decade^{-1} during the FU-Berlin time period, which is modest compared to the apparent strong weakening trends during subsets of the FU-Berlin time period. In particular, the long-term trend due to tropospheric expansion explains neither the maximum in the mid-1960s nor the minimum in the mid-2000s. KH13 proposed that the rapid weakening in QBO amplitude over the observational period was caused by global warming, just as global warming leads to QBO weakening in model simulations. However, it appears that the weakening during the observational period often outpaced that which is expected from global warming. The QBO weakening detected in KH13 and attributed to global warming had a rate of 6% decade^{-1}, double the rate expected from tropospheric expansion of 3% decade^{-1}.

e. The large internal variability of the QBO

The modest expected trends of QBO amplitude from global warming suggests that the large changes during the observational record resulted from internal variability. This previously unrecognized internal variability takes the form of decadal modulations of QBO amplitude in the buffer zone, where by "decadal" we refer to time scales much longer than the period of the QBO. The decadal variability is punctuated by two large deviations in QBO amplitude from its background levels: a maximum in the mid-1960s and a minimum in the mid-2000s (Fig. 8b). These decadal modulations are even discernible by eye in the radiosonde wind time series (Fig. 8a), where the size of the envelope containing the QBO winds fluctuates from a mid-1960s maximum to a mid-2000s minimum.

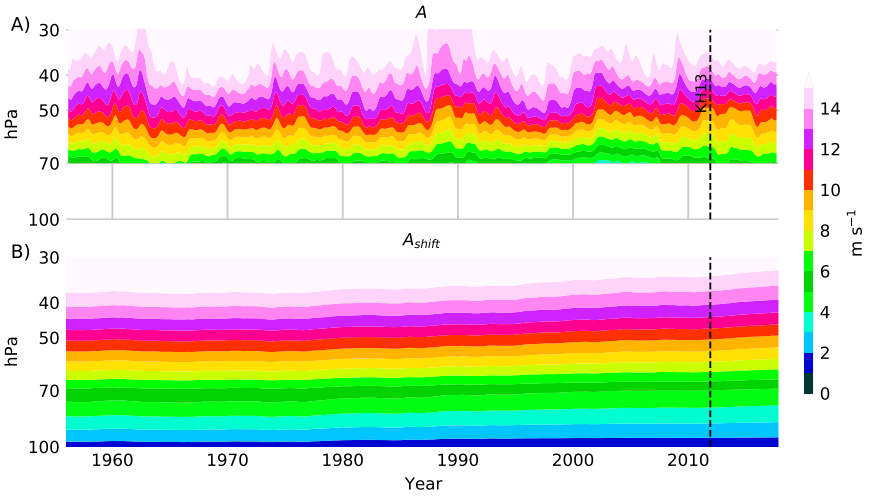

FIG. 7. (a) QBO amplitude (a) from FU-Berlin radiosonde dataset. (b) QBO amplitude predicted from tropospheric expansion (A_{shift}) using Eqs. (6) and 7. The reference QBO vertical structure $\overline{A}(p)$ is estimated as the time-average QBO amplitude in MERRA-2 using the zonal mean zonal winds along the equator over the period 1980–2020. The global average surface temperature anomaly $\delta T_s(t)$ is calculated using the Berkeley Earth global average surface temperature, subtracting the time average over the MERRA-2 period (1980–2020). The dashed line indicates the last QBO cycle used in the analysis of KH13 (October 2011). The physically expected trends can be seen to be much smaller than the variability.

Decadal modulation of QBO amplitude could modulate the strength of QBO teleconnections, for which the buffer zone is thought to be a key intermediary, and whose influence extends to the stratospheric polar vortex, midlatitude jet, and Madden–Julian oscillation (Holton and Tan 1982; Anstey and Shepherd 2014; Yoo and Son 2016; Dimdore-Miles et al. 2021). There is no theory explaining the mechanism behind this decadal modulation, nor how such modulation might impact the global teleconnections of the QBO. It is possible that the mid-2000s minimum could be related to a set of interconnected stratospheric dynamical transitions from the late 1990s to the early 2000s, including the sudden drop in stratospheric water vapor (e.g., Randel et al. 2006; Fueglistaler 2012), strengthening of the residual circulation, and increase in sudden stratospheric

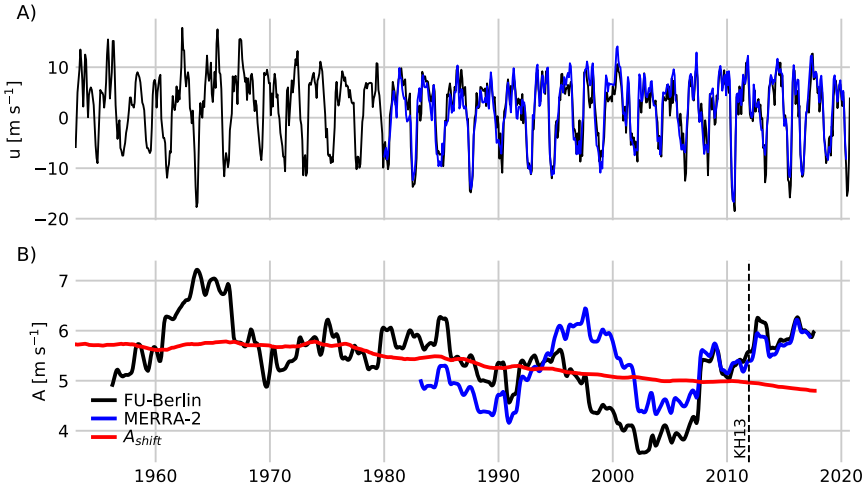

FIG. 8. (a) Zonal wind at 70 hPa from the FU-Berlin dataset (black), and zonal-mean zonal winds along the equator from MERRA-2 (blue). (b) QBO amplitude at 70 hPa. Horizontal slice from Fig. 7a of QBO amplitude in FU-Berlin at 70 hPa (black) and of Fig. 7b of A_{shift} at 70 hPa (red). QBO amplitude in MERRA-2 (blue). Vertical dashed line indicates the final QBO cycle used in KH13 (October 2011). The trend in A_{shift} cannot explain the low amplitude in the mid-2000s, from which the QBO has since recovered.

warmings (e.g., Butler et al. 2017). The relationships among these compositional and dynamical transitions, as well as their potential connections with the decadal modulation of QBO amplitude, remain to be clarified. The mid-1960s maximum in QBO amplitude also requires explanation, and it is not clear how insights gained from considering the anomalous dynamical transitions of the mid-2000s might bear on interpreting the mid-1960s amplitude maximum.

f. *Revisiting the detection of QBO amplitude trends at 70 hPa*

The weakening trend in $A(t, 70\text{ hPa})$ due to global warming over the observational period is estimated to have been about 3% decade^{-1}, not the 6% decade^{-1} reported in KH13 for the period 1953–2012 (nor the 11% decade^{-1} from 1976 to 2012 during the Singapore-only record). With the return of QBO amplitude to its long-term average since the mid-2000s, the observed weakening across the full period (1953–2020) is about 3.5% decade^{-1}. Does the correspondence between the expected and observed weakening trends of approximately 3% decade^{-1} support the conclusion in KH13 that a weakening trend has been detected? Or are there insufficient grounds to reject the null hypothesis of no linear trend?

We evaluate whether there are grounds to reject the null hypothesis that the QBO has exhibited no significant trend over the observational record 1953–2020. We use a 95% significance level. If the null hypothesis is rejected, then a trend has been detected, and the causal framework within this paper suggests that such a trend could be attributable to tropospheric expansion. If the null hypothesis is not rejected, then no trend has been detected, and no attribution of such a trend to global warming can be supported.

To test the null hypothesis, we estimate the possible trends that could have emerged in QBO amplitude due to random chance by using a bootstrapping approach in which synthetic QBO time series are generated with trends arising only due to noise. The synthetic QBO time series are generated by concatenating randomly sampled (with replacement) easterly and westerly half-cycles of the observed wind at 70 hPa, where a half-cycle of the QBO is defined as a contiguous period during which the deseasonalized zonal wind (smoothed with a 5-month running average) has the same sign. The westerly half-cycles average 15 months in duration and the easterly half-cycles average 10 months (the difference comes not from the mean wind speed, which has been averaged out by deseasonalizing, but from the asymmetry between easterly and westerly half cycles). We compute the amplitude as a function of time for these synthetic time series in the same manner as before, by taking the 72-month running standard deviation. The amplitude of the synthetic QBO has interannual variability of a similar magnitude (but with scrambled phasing) to that in the observed time series.

By construction, the synthetic time series have no persistence from half-cycle to half-cycle, and thus no expected trends on average. Therefore, amplitude trends of the synthetic QBO result from random chance in a manner arguably analogous to how half-cycle to half-cycle variability contributes noise to the observed trend. These amplitude trends due to half-cycle to half-cycle noise are then compared to the observed trends, where the observed trends also include contributions from low-frequency internal variability and global warming. The likelihoods of different slopes arising due to random chance are compared to the observed trend to estimate whether the observed trends significantly differ from zero. In particular, we are interested in calculating the two-sided probability that a slope at least as extreme as the observed -0.19 m s^{-1} decade^{-1} (over the period 1953–2020) could have occurred in the absence of a true long-term trend. We generate 10 000 synthetic time series and analyze the slopes of each. The synthetic slope distribution is approximately normal with mean -0.0004 m s^{-1} decade^{-1} (close to zero) and standard deviation -0.10 m s^{-1} decade^{-1}. In the 10 000 synthetic time series, there are 703 samples (7.03% of the total) with a slope with larger magnitude than the observed slope.

These results suggest that a trend comparable to or more extreme than has been observed arises about 7% of the time due to random chance from half-cycle to half-cycle. This statistical test fails to reject the null hypothesis at a 5% significance level. More years of continued weakening would be necessary for the agreement between the observed and theoretically expected trends to rise above the background noise. Our hypothesis test is strict in that it has not only failed to detect a significant trend due to global warming, but it has failed to detect a significant trend due to the combination of global warming *and* decadal internal variability. To the extent that the tropospheric expansion framework can be accepted as an estimator for the true global warming signal (as in Fig. 8b), the estimated trend has been reinforced due to internal variability by the mid-1960s maximum and the mid-2000s minimum. Thus, the half-cycle to half-cycle variability of the QBO obscures any trend in spite of the apparent reinforcement between global warming-induced weakening by the decadal internal variability.

4. Discussion

KH13 proposed that trends in QBO amplitude could constrain trends in residual mean upwelling (i.e., the advective component of the Brewer-Dobson circulation). The idea that trends in QBO amplitude could constrain trends in residual mean upwelling is based on the prevailing causal model for interpreting the relationship between upwelling and QBO amplitude—the upwelling hypothesis. The upwelling hypothesis holds that upwelling forms the buffer zone of the QBO, as argued by Saravanan (1990), who prescribed upwelling near the bottom of the 1D model of the QBO and reported the apparent formation of a buffer zone. KH13 applied the upwelling hypothesis to QBO amplitude trends, by arguing that a strengthening of upwelling in the lower stratosphere (as predicted in global warming simulations) was leading to a weakening of the QBO in the lower stratosphere (also predicted in global warming simulations). Then, considering the inverse problem, KH13 argued that observed weakening trends in the QBO could constrain trends in the upwelling, a variable much harder to measure than QBO amplitude. Upwelling trends have been subject to debate, in part because the robust

strengthening trends projected in global warming simulations (Butchart and Scaife 2001) and found in most atmospheric reanalyses (Abalos et al. 2015) appear to be inconsistent thus far, with some chemical proxies showing insignificant or weakening trends (e.g., Engel et al. 2017). An independent constraint on upwelling could help steer the debate, and KH13 proposed that the weakening of the QBO provided "strong support" for strengthening trends in upwelling, bolstering confidence that observed trends were consistent with model predictions. Because the present study has challenged both the detection of the trend and has adopted a framework other than the upwelling hypothesis, the present study has key implications for interpreting whether and how QBO amplitude constrains upwelling.

First, because this study detects no significant trend in observed QBO amplitude, this study has called into question whether observed QBO amplitude *presently* constrains trends in upwelling. But, even if this study had detected a trend in observed QBO amplitude, the tropospheric expansion framework suggests that QBO amplitude trends might *never* constrain trends in upwelling. Rather than interpreting lower stratospheric changes using the upwelling hypothesis, this paper has used the tropospheric expansion framework. In the tropospheric expansion framework, upwelling and QBO amplitude are expected to respond in a correlated way to global warming, but in a way that does not necessarily reveal their causal relationships because their changes are confounded by tropospheric expansion. Thus, within the tropospheric expansion framework, the response of upwelling and QBO amplitude does not depend on any causal relationship that upwelling and QBO amplitude might possess in the basic state, nor can the response reveal the nature of such basic state causal relationships.

It is important to note that the tropospheric expansion framework is not in conflict with the upwelling hypothesis; rather, any success of the tropospheric expansion framework provides neither support nor refutation of the upwelling hypothesis. Consider on the one hand if the upwelling hypothesis were correct: then, given that upwelling obeys the expectations of tropospheric expansion [as demonstrated in Oberländer-Hayn et al. (2016)], changes in QBO amplitude would be proximally controlled by upwelling but ultimately also consistent with tropospheric expansion. Consider on the other hand if the upwelling hypothesis were incorrect: then, as long as the process that does in fact form the buffer zone obeys the expectations of tropospheric expansion, changes in QBO amplitude would be proximally controlled by the buffer zone formation process but still ultimately consistent with tropospheric expansion. In this latter case, there would still be a correlation between upwelling and QBO amplitude due to confounding by tropospheric expansion. Therefore, trends in QBO amplitude due to global warming can neither support nor refute the upwelling hypothesis nor any other buffer zone formation mechanism.

Even if one gains high confidence in the buffer zone formation process, the tropospheric expansion framework suggests that trends in QBO amplitude are unlikely to provide a targeted and independent constraint on trends in that formation process. This is because tropospheric expansion will lead to many confounded changes, which can ultimately be understood in terms of the robust thermodynamical effects of global warming. Therefore, trends in QBO amplitude in the lower stratosphere might be interpreted not as providing a targeted constraint on the particular dynamical processes relevant to the QBO, but rather as providing one of many highly correlated constraints on the robust thermodynamical effects of global warming. These robust thermodynamical effects can be measured confidently in terms of the surface temperature or radiative diagnostics in the vicinity of the tropopause, and can be related with some confidence to tropospheric expansion through the tropospheric expansion scaling (as shown in section 2b). Therefore, rather than providing a targeted constraint on trends in its governing processes, trends in QBO amplitude might represent just one or many confounded trends in atmospheric variables, some of which might be dynamically connected in the basic state, many or all of whose trends are thermodynamically connected through tropospheric expansion, but none of which provide a targeted constraint on the trends of the others.

5. Conclusions

We have derived a simple scaling that relates the tropospheric depth to other thermodynamical variables under basic assumptions of a moist adiabatic tropical temperature profile, fixed surface relative humidity, and fixed temperature at the top of the troposphere. This scaling relationship predicts that the troposphere deepens in response to global warming at a rate of approximately 6 hPa K^{-1}. This tropospheric depth scaling is in good agreement with output from five global climate models, which showed that radiative metrics for the tropospheric depth closely followed the theoretical scaling.

The tropospheric depth scaling was then employed to develop a physical expectation for trends in QBO amplitude in the buffer zone. The QBO amplitude profile in 12 CMIP6 GCMs was shown to ascend in response to global warming in a manner quantitatively consistent with the predictions from tropospheric expansion given each model's rate of warming and basic state QBO profile. A previous study reported to have detected significant weakening trends in QBO amplitude at 70 hPa (in the buffer zone), and these trends were attributed to global warming (Kawatani and Hamilton 2013). This weakening trend remains the only aspect of the QBO for which proposed changes due to global warming have been detected and attributed. However, our results call into question this detection and attribution. Although the QBO amplitude in the buffer zone is expected to decrease with global warming, it appears that the previously large rate of decrease into the mid-2000s exceeded by at least a factor of 2 the rate that which had been predicted by tropospheric expansion, and has since been followed by a recovery in QBO amplitude. At this time, the trends in QBO amplitude at 70 hPa are not statistically significantly different from zero.

Our work draws attention to the hitherto underappreciated large internal variability in QBO amplitude at 70 hPa. This internal variability precludes the detection of a trend due to global warming. This internal variability could modulate the

strength of QBO teleconnections, for which the buffer zone is thought to be a key region, and which exert influence throughout the globe.

Acknowledgments. The authors acknowledge constructive reviews from Kevin Hamilton and two anonymous reviewers, as well as helpful conversations with Benjamin Schaffer and Nathaniel Tarshish. This report was prepared by A.M. under Award NA18OAR4320123 from the National Oceanic and Atmospheric Administration, U.S. Department of Commerce. The statements, findings, conclusions, and recommendations are those of the authors and do not necessarily reflect the views of the National Oceanic and Atmospheric Administration, or the U.S. Department of Commerce.

Data availability statement. QBO radiosonde data are freely available from the Freie Universität Berlin: https://www.geo.fu-berlin.de/en/met/ag/strat/produkte/qbo/index.html. MERRA-2 data are freely available from the NASA Earthdata portal: https://disc.gsfc.nasa.gov/datasets?project=MERRA-2. Berkeley Earth global temperature time series are freely available at http://berkeleyearth.org/data/. CMIP6 data are freely available from the Earth System Grid Federation: https://esgf-node.llnl.gov/search/cmip6/.

REFERENCES

Abalos, M., B. Legras, F. Ploeger, and W. J. Randel, 2015: Evaluating the advective Brewer-Dobson circulation in three reanalyses for the period 1979–2012. *J. Geophys. Res. Atmos.*, **120**, 7534–7554, https://doi.org/10.1002/2015JD023182.

Anstey, J. A., and T. G. Shepherd, 2014: High-latitude influence of the quasi-biennial oscillation. *Quart. J. Roy. Meteor. Soc.*, **140** (678), 1–21, https://doi.org/10.1002/qj.2132.

Baldwin, M. P., and Coauthors, 2001: The quasi-biennial oscillation. *Rev. Geophys.*, **39**, 179–229, https://doi.org/10.1029/1999RG000073.

Boer, G. J., 1993: Climate change and the regulation of the surface moisture and energy budgets. *Climate Dyn.*, **8**, 225–239, https://doi.org/10.1007/BF00198617.

Butchart, N., 2014: The Brewer-Dobson circulation. *Rev. Geophys.*, **52**, 157–184, https://doi.org/10.1002/2013RG000448.

——, and A. A. Scaife, 2001: Removal of chlorofluorocarbons by increased mass exchange between the stratosphere and troposphere in a changing climate. *Nature*, **410**, 799–802, https://doi.org/10.1038/35071047.

——, and Coauthors, 2006: Simulations of anthropogenic change in the strength of the Brewer–Dobson circulation. *Climate Dyn.*, **27**, 727–741, https://doi.org/10.1007/s00382-006-0162-4.

——, J. A. Anstey, Y. Kawatani, S. M. Osprey, J. H. Richter, and T. Wu, 2020: QBO changes in CMIP6 climate projections. *Geophys. Res. Lett.*, **47**, 2019GL086903, https://doi.org/10.1029/2019GL086903.

Butler, A. H., J. P. Sjoberg, D. J. Seidel, and K. H. Rosenlof, 2017: A sudden stratospheric warming compendium. *Earth Syst. Sci. Data*, **9**, 63–76, https://doi.org/10.5194/essd-9-63-2017.

Chapman, S., 1930: A theory of upper atmospheric ozone. *Mem. Roy. Meteor. Soc.*, **3**, 103–125.

Dimdore-Miles, O., L. Gray, and S. Osprey, 2021: Origins of multi-decadal variability in sudden stratospheric warmings. *Wea. Climate Dyn.*, **2**, 205–231, https://doi.org/10.5194/wcd-2-205-2021.

Dunkerton, T. J., and D. P. Delisi, 1985: Climatology of the equatorial lower stratosphere. *J. Atmos. Sci.*, **42**, 376–396, https://doi.org/10.1175/1520-0469(1985)042<0376:COTELS>2.0.CO;2.

Engel, A., H. Bönisch, M. Ullrich, R. Sitals, O. Membrive, F. Danis, and C. Crevoisier, 2017: Mean age of stratospheric air derived from AirCore observations. *Atmos. Chem. Phys.*, **17**, 6825–6838, https://doi.org/10.5194/acp-17-6825-2017.

Fueglistaler, S., 2012: Stepwise changes in stratospheric water vapor? *J. Geophys. Res.*, **117**, D13302, https://doi.org/10.1029/2012JD017582.

Garcia, R. R., and W. J. Randel, 2008: Acceleration of the Brewer–Dobson circulation due to increases in greenhouse gases. *J. Atmos. Sci.*, **65**, 2731–2739, https://doi.org/10.1175/2008JAS2712.1.

Gelaro, R., and Coauthors, 2017: The Modern-Era Retrospective Analysis for Research and Applications, version 2 (MERRA-2). *J. Climate*, **30**, 5419–5454, https://doi.org/10.1175/JCLI-D-16-0758.1.

GMAO, 2015a: MERRA-2 tavgM_3d_rad_Np: 3d, Monthly mean, Time-Averaged, Pressure-Level, Assimilation, Radiation Diagnostics V5.12.4. Goddard Earth Sciences Data and Information Services Center (GES DISC), accessed February 2021, https://doi.org/10.5067/H3YGROBVBGFJ.

——, 2015b: MERRA-2 tavgM_3d_tdt_Np: 3d, Monthly mean, Time-Averaged, Pressure-Level, Assimilation, Temperature Tendencies V5.12.4. Goddard Earth Sciences Data and Information Services Center (GES DISC), accessed January 2021, https://doi.org/10.5067/VILT59HI2MOY.

Hartmann, D. L., and K. Larson, 2002: An important constraint on tropical cloud–climate feedback. *Geophys. Res. Lett.*, **29**, 1951, https://doi.org/10.1029/2002GL015835.

Holton, J. R., and H.-C. Tan, 1982: The quasi-biennial oscillation in the Northern Hemisphere lower stratosphere. *J. Meteor. Soc. Japan*, **60**, 140–148, https://doi.org/10.2151/jmsj1965.60.1.140.

Jeevanjee, N., and S. Fueglistaler, 2020: Simple spectral models for atmospheric radiative cooling. *J. Atmos. Sci.*, **77**, 479–497, https://doi.org/10.1175/JAS-D-18-0347.1.

Kawatani, Y., and K. Hamilton, 2013: Weakened stratospheric quasibiennial oscillation driven by increased tropical mean upwelling. *Nature*, **497**, 478–481, https://doi.org/10.1038/nature12140.

Kuang, Z., and D. L. Hartmann, 2007: Testing the fixed anvil temperature hypothesis in a cloud-resolving model. *J. Climate*, **20**, 2051–2057, https://doi.org/10.1175/JCLI4124.1.

Lorenz, D. J., and E. T. DeWeaver, 2007: Tropopause height and zonal wind response to global warming in the IPCC scenario integrations. *J. Geophys. Res.*, **112**, https://doi.org/10.1029/2006JD008087.

Match, A., and S. Fueglistaler, 2019: The buffer zone of the quasi-biennial oscillation. *J. Atmos. Sci.*, **76**, 3553–3567, https://doi.org/10.1175/JAS-D-19-0151.1.

——, and ——, 2020: Mean flow damping forms the buffer zone of the quasi-biennial oscillation: 1D theory. *J. Atmos. Sci.*, **77**, 1955–1967, https://doi.org/10.1175/JAS-D-19-0293.1.

——, and ——, 2021: Anomalous dynamics of QBO disruptions explained by 1D theory with external triggering. *J. Atmos. Sci.*, **78**, 373–383, https://doi.org/10.1175/JAS-D-20-0172.1.

Newman, P. A., L. Coy, S. Pawson, and L. R. Lait, 2016: The anomalous change in the QBO in 2015–2016. *Geophys. Res. Lett.*, **43**, 8791–8797, https://doi.org/10.1002/2016GL070373.

Oberländer-Hayn, S., and Coauthors, 2016: Is the Brewer-Dobson circulation increasing, or moving upward? *Geophys. Res. Lett.*, **43**, 1772–1779, https://doi.org/10.1002/2015GL067545.

Randel, W. J., F. Wu, H. Vömel, G. E. Nedoluha, and P. Forster, 2006: Decreases in stratospheric water vapor after 2001: Links to changes in the tropical tropopause and the Brewer-Dobson circulation. *J. Geophys. Res.*, **111**, D12312, https://doi.org/10.1029/2005JD006744.

Richter, J. H., and Coauthors, 2020: Response of the quasi-biennial oscillation to a warming climate in global climate models. *Quart. J. Roy. Meteor. Soc.*, https://doi.org/10.1002/qj.3749, in press.

Saravanan, R., 1990: A multiwave model of the quasi-biennial oscillation. *J. Atmos. Sci.*, **47**, 2465–2474, https://doi.org/10.1175/1520-0469(1990)047⟨2465:AMMOTQ⟩2.0.CO;2.

Schenzinger, V., S. Osprey, L. Gray, and N. Butchart, 2017: Defining metrics of the quasi-biennial oscillation in global climate models. *Geosci. Model Dev.*, **10**, 2157–2168, https://doi.org/10.5194/gmd-10-2157-2017.

Seeley, J. T., N. Jeevanjee, and D. M. Romps, 2019: FAT or FiTT: Are anvil clouds or the tropopause temperature invariant? *Geophys. Res. Lett.*, **46**, 1842–1850, https://doi.org/10.1029/2018GL080096.

Shepherd, T. G., 2014: Atmospheric circulation as a source of uncertainty in climate change projections. *Nat. Geosci.*, **7**, 703–708, https://doi.org/10.1038/ngeo2253.

——, and C. McLandress, 2011: A robust mechanism for strengthening of the Brewer–Dobson circulation in response to climate change: Critical-layer control of subtropical wave breaking. *J. Atmos. Sci.*, **68**, 784–797, https://doi.org/10.1175/2010JAS3608.1.

Singh, M. S., and P. A. O'Gorman, 2012: Upward shift of the atmospheric general circulation under global warming: Theory and simulations. *J. Climate*, **25**, 8259–8276, https://doi.org/10.1175/JCLI-D-11-00699.1.

Tompkins, A. M., and G. C. Craig, 1999: Sensitivity of tropical convection to sea surface temperature in the absence of large-scale flow. *J. Climate*, **12**, 462–476, https://doi.org/10.1175/1520-0442(1999)012<0462:SOTCTS>2.0.CO;2.

Vallis, G. K., P. Zurita-Gotor, C. Cairns, and J. Kidston, 2015: Response of the large-scale structure of the atmosphere to global warming. *Quart. J. Roy. Meteor. Soc.*, **141**, 1479–1501, https://doi.org/10.1002/qj.2456.

Yoo, C., and S.-W. Son, 2016: Modulation of the boreal wintertime Madden–Julian Oscillation by the stratospheric quasi-biennial oscillation. *Geophys. Res. Lett.*, **43**, 1392–1398, https://doi.org/10.1002/2016GL067762.